REALISTIC ANTENNA ELEMENTS AND DIFFERENT ARRAY TOPOLOGIES IN THE DOWNLINK OF UMTS-FDD NETWORKS

S. Bieder, L. Häring, A. Czylwik, P. Paunov

Department of Communication Systems
University of Duisburg-Essen
Bismarckstr. 81
47057 Duisburg, Germany
bieder@nts.uni-duisburg-essen.de

B. K. Chalise

Communication and Remote Sensing Lab.
Université catholique de Louvain
Place du Levant, 2
B-1348 Louvain-La-Neuve, Belgium
chalise@tele.ucl.ac.be

ABSTRACT

Prior investigations have shown that the capacity of a UMTS-FDD network can be highly improved by employing antenna arrays at the base station side and utilizing beamforming. The amount of capacity improvement, which can be achieved, strongly depends on the number of antenna elements in the array, the array topology as well as the characteristics of the single antenna element. Therefore, close-to-reality investigations on the network capacity must incorporate realistic antenna element characteristics. In this contribution, a UMTS-FDD network equipped with smart antennas at the base stations is analysed on system level to gain insight on the effect of different realistic antenna and array characteristics on the network capacity. For this purpose, different types of antenna elements like dipole and commercially available real-world base station antennas for UMTS are compared for different array topologies.

1. INTRODUCTION

The capacity of 3rd generation mobile communication systems is limited by the amount of interference in the network. The level of interference can be decreased by using smart antennas together with beamforming which achieves capacity enhancement and range extension [1]. Thereby, the configuration of the antenna array as well as the design of the antenna elements in the array affects the performance of the network. In [2], different antenna characteristics and typical array configurations have been intensively investigated. These studies have been carried out in a static two-dimensional environment such that the obtained results are valid for snapshots in a non-correlated scenario. Furthermore, the impact of the elevation angle can not be analysed in a two dimensional scenario. In this contribution, these studies are extended to a dynamic three dimensional scenario such that both, the influences of the azimuth angle as well as the elevation angle are incorporated. The network capacity is investigated on system level for different array topologies and compared for idealized antenna elments as well as commercially available real world base station antennas. The simulations are carried out in dynamic scenarios such that time correlation of propagation parameters is taken into account to get a more realistic insight.

2. SIMULATION CONCEPT

The simulator focusses on the downlink of the transmission due to the fact that the traffic load in the downlink in comparison with the uplink of the transmission is much higher. Hence, the overall system capacity is limited by this link direction. For investigations on the entire capacity of a cellular network, only simulations based on a system level can be reasonably performed due to complexity reasons. The dynamic system level simulator which is used in this paper has been presented in [3] in detail. It incorporates handover aspects, power control and user mobility. Broadcast channels like the Common Pilot Channel (CPICH) as well as dedicated channels like the Dedicated Physical Data Channel (DPDCH) are implemented in the simulator.

2.1. Simulation Structure

A realistic dynamic behaviour of the simulator is achieved by the usage of strongly correlated time snapshots. In each snapshot, the position of the mobile stations, the traffic situation and the channels between the mobile stations and base stations are either calculated newly or updated. All of these parameters are described by stochastic processes. The mobility of the mobile stations is modelled by a random walk process while the traffic situation of the mobile stations is described by a Poisson process. The stochastic multipath channel model includes effects of distance attenuation, attenuation due to excess delay and log-normal fading of the direct path as well as the reflected paths. After the calculation of these parameters, mobile stations are preassigned to

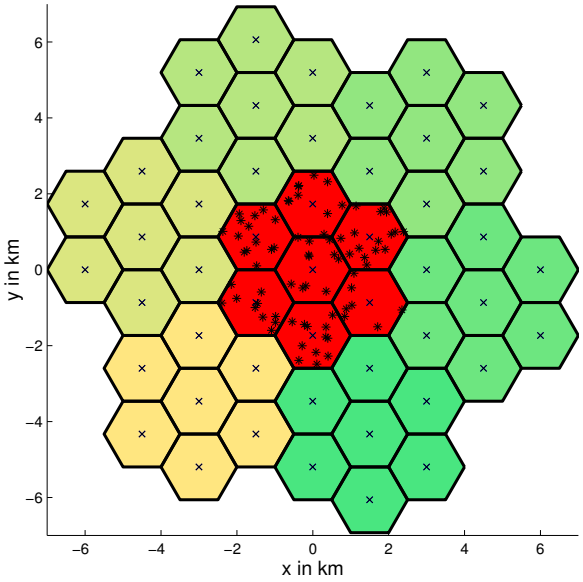

Fig. 1. Locations of base and mobile stations.

base stations based upon the received pilot channel power. Downlink beamforming is carried out for the DPDCH channel. The signal-to-interference-and-noise power ratio (SINR) values for the DPDCH and CPICH channels are calculated at each mobile station. An iterative fast closed-loop power control method is used to adjust the powers of DPDCH channels. The mobile stations that cannot be provided with the target SINR for DPDCH are considered to be in outage. A more detailed description of the simulation concept is given in [3].

2.2. Network Topology

A cellular configuration consisting of a main cluster and six surrounding areas is created as shown in Fig. 1.

In order to enhance the computational speed of the simulator, a wrap-around technique is used such that the parameters of the mobile stations are to be calculated only within the main area in the center. The other areas are periodical copies of the main area and are used to create a realistic interference scenario inside the main area. Each area consists of a central hexagonal cell surrounded by six other hexagonal cells. Each cell has a single Base Station (BS) at its centre. Before the first snapshot is calculated, Mobile Stations (MS) are distributed uniformly within the main area.

The considered UMTS Terrestial Radio Access (UTRA) standard is based on the Wideband Code Division Multiple Access (WCDMA) technology. In the downlink of a WCDMA system, users assigned to the same base station are separated by the spreading codes. The Orthogonal Variable Spreading Factor (OVSF) codes with spreading factors between 4 and 512 are available in WCDMA, depending on the data rate that a mobile station requests for. Therefore, a simplified code administration method is incorporated which takes into account a limited number of different spreading codes in the downlink. According to this, mobile stations can only be assigned to base stations if a code is available. It is assumed that a base station uses a single scrambling code. In the dynamic simulator, the code administration method can be activated or deactivated according to parameters chosen by the user. in this paper, the effect of code limitation is not considered in order to analyse the impact of the antenna and antenna array design in a network where the network capacity is merely interference limited.

3. ANTENNA MODEL

The antenna model is derived following the calculations in [4] in a more general way. It is assumed that the element spacing in the array is sufficient such that no coupling effects have to be considered. The antenna array at the base station consists of M identical elements. The reference antenna element which is needed for the calculation of the entire array radiation pattern is located in the origin. It is considered to have a field radiation pattern $E_0(\theta, \varphi)$ which is a function of the azimuth angle φ as well as the elevation angle θ. The m-th element of the antenna array is located at the position $\vec{r}_m = (x_{0,m},\ y_{0,m},\ z_{0,m})^{\mathrm{T}}$ and is spatially aligned in the azimuth and elevation direction $\Delta\varphi_m$ and $\Delta\theta_m$, respectively, such that the field radiation pattern of the m-th antenna element is given by:

$$E_m(\theta, \varphi) = E_0(\theta - \Delta\theta_m, \varphi - \Delta\varphi_m) \cdot c_m(\theta, \varphi). \quad (1)$$

Here, the complex factor $c_m(\theta, \varphi)$ of m-th element describes the impact of the displacement of the element relative to the reference antenna element. This displacement results in a phase difference $\Delta_m(\theta, \varphi)$ of the impinging or radiated signals:

$$\begin{aligned} \Delta_m(\theta, \varphi) \quad = \quad & x_{0,m} \sin(\theta) \cos(\varphi) + y_{0,m} \sin(\theta) \sin(\varphi) \\ & + z_{0,m} \cos(\theta) \end{aligned} \quad (2)$$

such that the complex factor of the m-th element for a specific frequency ω can be written as:

$$c_m(\theta, \varphi) = \exp(+\mathrm{j}\ k \cdot \Delta_m(\theta, \varphi)) \text{ with } k = \omega \cdot \sqrt{\mu_0 \varepsilon_0}. \quad (3)$$

4. DOWNLINK BEAMFORMING

A spatial covariance matrix based beamforming method is performed for the dedicated channels in UMTS.

4.1. Covariance Matrix Calculation

For the link between the i-th mobile station and the j-th base station, the simulator takes the strongest Q_{ij} paths into account. Assuming all paths $l = 1 \ldots Q_{ij}$ are uncorrelated, the

ideal spatial covariance matrix (averaged over fast fading) can be approximated by [6]

$$\mathbf{R}_{ij} = \sum_{l=1}^{Q_{ij}} A_{ijl}^2 \cdot \mathbf{a}\left(\theta_{ijl}, \varphi_{ijl}\right) \cdot \mathbf{a}^{\mathrm{H}}\left(\theta_{ijl}, \varphi_{ijl}\right), \qquad (4)$$

where $A_{ijl}^2 = 10^{-\frac{L_{ijl}}{10}}$ can be interpreted as an estimate of the medium-term expectation of the transmission factor A_{ijl}^2 corresponding to the wave of path l. In (4), $\mathbf{a}\left(\varphi_{ijl}, \theta_{ijl}\right)$ denotes the array response vector of a wave incident at the base station with the azimuth angle φ_{ijl} and the elevation angle θ_{ijl}. The array response vector $\mathbf{a}\left(\varphi_{ijl}, \theta_{ijl}\right)$ of an antenna array consisting of M elements can be written in terms of the element field radiation patterns:

$$\mathbf{a}\left(\theta_{ijl}, \varphi_{ijl}\right) = \left[E_1\left(\theta_{ijl}, \varphi_{ijl}\right), \ \ldots, \ E_M\left(\theta_{ijl}, \varphi_{ijl}\right)\right]^{\mathrm{T}}. \qquad (5)$$

For the simulations, we assume perfect knowledge of all Directions of Arrival (DoAs) and average path attenuations in the downlink. The covariance matrix in the downlink can be obtained by estimating the average spatial covariance matrix in the uplink and transforming it to the downlink frequency [5].

4.2. Beamforming Algorithm

Consider the i_0-th mobile station which is linked to N_{i_0} different base stations. The index of these base stations linked to mobile station i_0 is denoted as $j_k(i_0)$ with $k = 1 \ldots N_{i_0}$. The covariance matrix based beamforming algorithm maximizes for each link the average desired signal power P_{S,i_0} received by the mobile station i_0 while keeping the sum of the total generated interference powers $P_{\mathrm{I},i\neq i_0}$ at all undesired mobile stations constant [3]. The solution of this maximization problem is the weight vector for the considered link.

$$\mathbf{w}^{(i_0,j_k(i_0))} = \left[w_1^{(i_0,j_k(i_0))}, w_2^{(i_0,j_k(i_0))}, \ldots w_M^{(i_0,j_k(i_0))}\right]^{\mathrm{H}}, \qquad (6)$$

where $w_m^{(i_0,j_k(i_0))}$ is the complex weight factor of the m-th antenna element for the link (BS $j_k(i_0) \rightarrow$ MS i_0) and $(\cdot)^{\mathrm{H}}$ denotes the Hermetian transpose operator. The data signal $s^{(i_0,j_k(i_0))}(t)$ for the i_0-th mobile station is transmitted in parallel over the M antenna elements of the antenna array using the calculated weight vector $\mathbf{w}^{(i_0,j_k(i_0))}$. The superposition of all radiated fields of all elements results in the total radiated field of the entire array for this link

$$\begin{aligned} E_{\mathrm{tot}}^{(i_0,j_k(i_0))}(\theta,\varphi,t) &= s^{(i_0,j_k(i_0))}(t) \\ &\quad \cdot \sum_{m=1}^{M} w_m^{(i_0,j_k(i_0))} \cdot E_m(\theta,\varphi). \end{aligned} \qquad (7)$$

The data signal is assumed to be normalized such that for the power P_{s} of all data signals is normalized such that it holds

$$P_{\mathrm{s}}^{(i_0,j_k(i_0))} = \mathrm{E}\left\{s^{(i_0,j_k(i_0))}(t) \cdot \left(s^{(i_0,j_k(i_0))}(t)\right)^*\right\} = 1. \qquad (8)$$

Using the free space wave impedance $Z_{\mathrm{F}} = 377\ \Omega$, the radiation intensity for the considered link can be determined by

$$\begin{aligned} U^{(i_0,j_k(i_0))}(\theta,\varphi) &= \frac{1}{2\,Z_{\mathrm{F}}} \cdot \mathrm{E}\Big\{E_{\mathrm{tot}}^{(i_0,j_k(i_0))}(\theta,\varphi,t) \\ &\quad \cdot \left(E_{\mathrm{tot}}^{(i_0,j_k(i_0))}(\theta,\varphi,t)\right)^* \Big\}. \end{aligned} \qquad (9)$$

Hence, the total radiated power P_{rad} for the considered link can be calculated by an integration in spherical coordinates over the according radiation intensity $U(\theta,\varphi)$

$$\begin{aligned} P_{\mathrm{rad}}^{(i_0,j_k(i_0))} &= \int_{\varphi=0}^{2\pi}\int_{\theta=0}^{\pi} U^{(i_0,j_k(i_0))}(\theta,\varphi) \cdot \sin(\theta)\,\mathrm{d}\theta\,\mathrm{d}\varphi \\ &= \sum_{\nu=1}^{M}\sum_{\mu=1}^{M} w_\nu^{(i_0,j_k(i_0))} \cdot w_\mu^{(i_0,j_k(i_0))^*} \cdot I_{\nu\mu} \end{aligned} \qquad (10)$$

$$\begin{aligned} I_{\nu\mu} &= \frac{1}{2\,Z_{\mathrm{F}}} \int_{\varphi=0}^{2\pi}\int_{\theta=0}^{\pi} E_\nu(\theta,\varphi) \cdot E_\mu^*(\theta,\varphi) \\ &\quad \cdot \sin(\theta)\,\mathrm{d}\theta\,\mathrm{d}\varphi \end{aligned} \qquad (11)$$

The antenna elements of the antenna array are assumed to be lossless. Hence, the field radiation patterns of the antenna elements are normalized in such a way, that it holds $I_{mm} = 1$.

Using the corresponding field radiation pattern of the basis antenna element, beamforming can be performed for arbitrary antenna types and array topologies.

5. ANTENNA ELEMENTS AND ARRAY TOPOLOGIES

The main focus of this work lies on the influence of different element numbers M as well as different element characteristics on the network capacity. Furthermore, the influence of the array topology, i.e. the location of the antenna elements in the antenna array, is investigated. The number of users which can be served with a certain quality of service is used as a measure for the network capacity.

Dipole antennas with omnidirectional radiation characteristic in the azimuth plane as well as commercially available real world sector base station antennas for UMTS networks [7] are used as basis antenna elements (type: KATHREIN, model: 80010270). For the real world sector antennas, the half-power beam width in the azimuth plane is approximately

60° while in the elevation plane it is approximately 6.5°. Furthermore, an idealized antenna element is used in the simulations which has the realistic radiation characteristic of the real world sector antenna in elevation direction but an omnidirectional radiation characteristic in azimuth direction. In the following, this antenna type is named as non-sectorized with realistic downtilt angle (DTA). The DTA of the sectorized antenna and the non-sectorized antenna with realistic downtilt angle can be set in the range (0°- 10°). The normalized radiation patterns of the investigated antennas are illustrated in Fig. 2. Here, the DTA of the sectorized antenna as well as the non-sectorized antenna with realistic downtilt angle is set to 5°. The antenna gains of the sector antenna, the dipole antenna and the non-sectorized antenna with realistic downtilt angle are $G_{\mathrm{S}} \approx 18$ dBi, $G_{\mathrm{D}} = 1.5$ dBi and $G_{\mathrm{NS}} \approx 10$ dBi, respectivly.

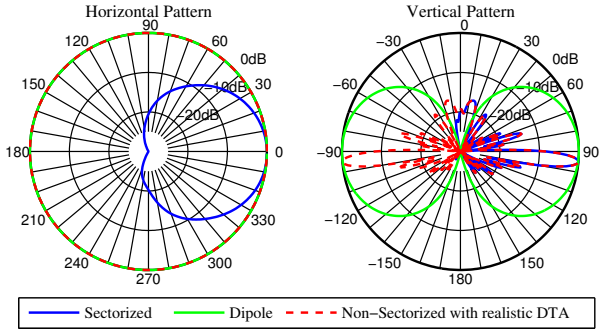

Fig. 2. Two-dimensional radiation patterns for the three investigated antenna types.

Designing an antenna array, the antenna spacing must be chosen sufficiently high to avoid mutual coupling between the antenna elements as mentioned in section 3. Hence, for the following investigations the antenna spacing is chosen to $d = 3\ \lambda_{\mathrm{DL}}$, where $\lambda_{\mathrm{DL}} = 14$ cm denotes the wavelength according the the UMTS-FDD DL center frequency of $f_{\mathrm{DL}} = 2140$ MHz.

To gain insight of the impact of the array design on system level, three different array topologies are compared by simulations:

1. Uniform Circular Array (UCA)
   located in the horizontal (x, y)-plane,

2. Uniform Linear Array (ULA)
   located in the horizontal (x, y)-plane,

3. Uniform Linear Array
   located in the (y, z)-plane.

Fig. 3 shows for an examplary UCA consisting of $M = 10$ elements the antenna position as well as the alignment of the antenna which is illustrated by the the according horizontal radiation patterns of the antenna elements.

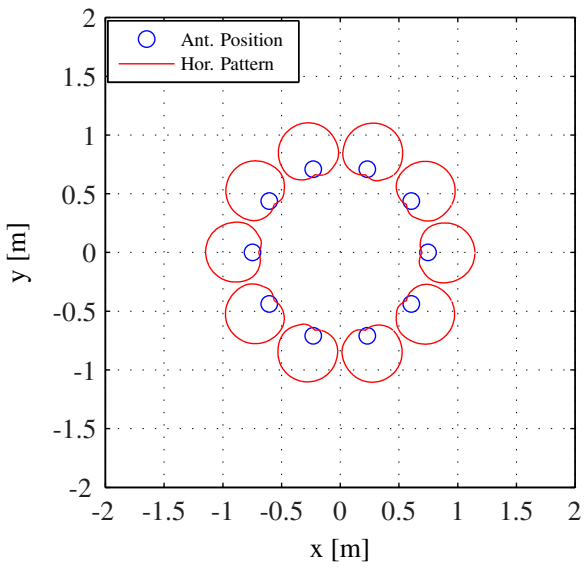

Fig. 3. Antenna positions and aligned horizontal radiation patterns of a UCA located in the (x, y)-plane for an examplary array consisting of $M = 10$ antennas.

The antenna position of an examplary ULA located in the (x, y)-plane and consisting of $M = 10$ elements is shown in Fig. 4. The according horizontal radiation patterns of the antenna elements demonstrate the alignment antenna elements. The antenna elements are aligned such that the entire azimuth range can be covered.

Referring to Fig. 5, the antenna elements of the array are located equally spaced on the straight line $z = y$ for a ULA located in the (y, z)-plane.

For this array topology, the antenna elements are again aligned such that the entire azimuth range can be covered which is illustrated by the projection of the antenna positions and horizontal patterns to the (x, y)-plane as shown in Fig. 6. Since the antenna position coordinate $z_{0,m}$ increases with the element index m for a ULA located in the (y, z)-plane, beamforming can be performed in elevation direction in addition to the azimuth direction for this array configuration. Because the ULA located in the (y, z)-plane is not a planar array, the beamforming in elevation direction can not be performed independently to the beamforming in the azimuth direction [4].

For a ULA located in the (y, z)-plane the alignment of the antenna elements in elevation direction (i.e. the DTA) is not changed with respect to the according alignment in elevation direction for a UCA or a ULA located in the (x, y)-plane.

6. SIMULATION RESULTS

For each simulation, all potential users in the network are inactive at the begin of the simulation. In each snapshot, a number of inactive users defined by the average call arrival

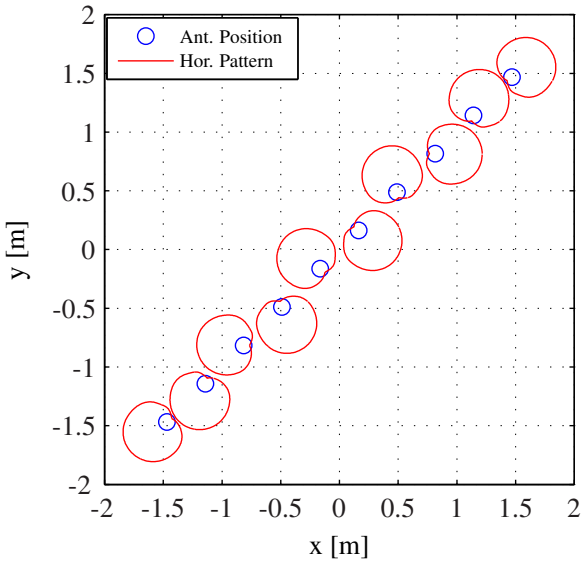

Fig. 4. Antenna positions and aligned horizontal radiation pattern of a ULA located in the (x, y)-plane for an examplary array consisting of $M = 10$ antennas.

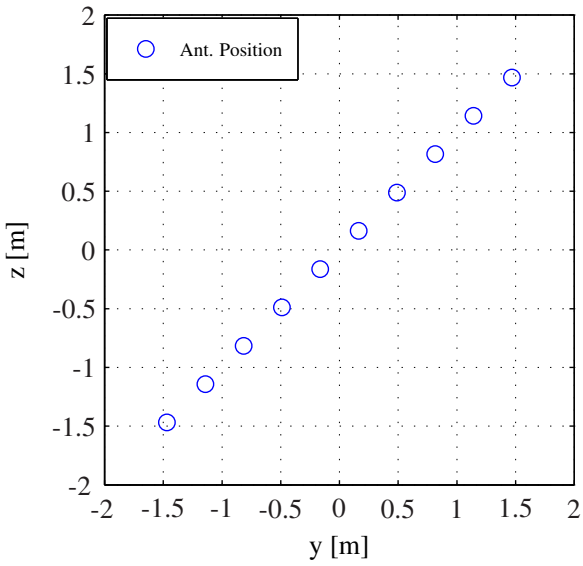

Fig. 5. Antenna positions of a ULA located in the (y, z)-plane for an examplary array consisting of $M = 10$ antennas.

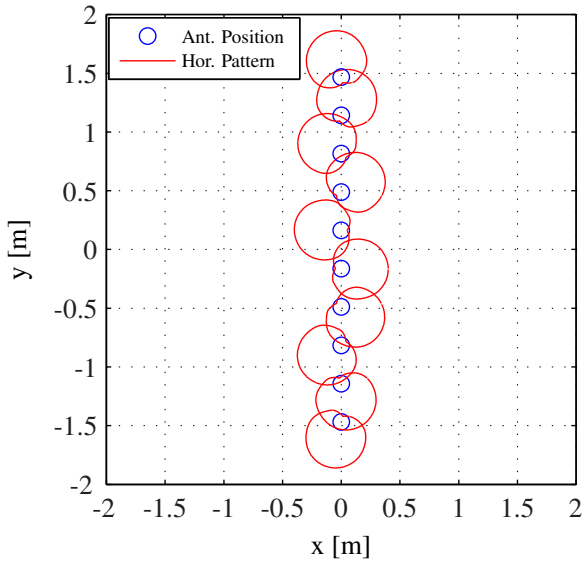

Fig. 6. Antenna positions and aligned horizontal radiation pattern of a ULA located in the (y, z)-plane for an examplary array consisting of $M = 10$ antennas.

rate tries to establish a connection with a certain quality of service. The requested connections are accepted and hold until the amount interference power in the network exceeds a certain level. This results in a number of served users that increases in average with time from zero to a certain saturation value. The exact behaviour changes with each simulated realization due to the different random parameters describing the channel state, the traffic situation and the user location. Fig. 7 shows three distinct realizations for a simulation of a network where the BSs are equipped with a UCA consisting of 9 dipole antennas. For each investigated scenario, the average

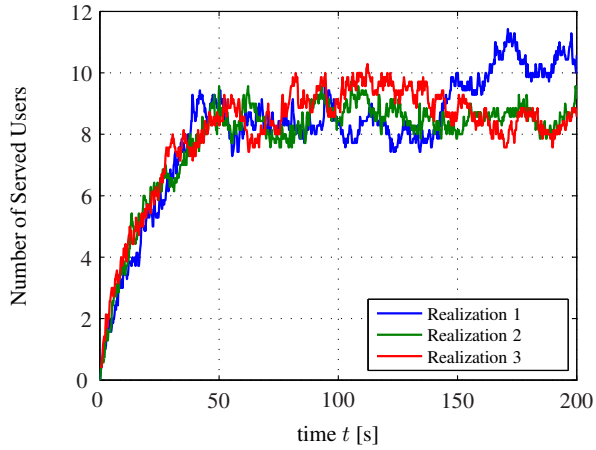

Fig. 7. Number of servable users versus time for three examplary realizations for a UCA consisting of 9 dipole antennas.

number of servable users is determined by averaging over a sufficient number of simulated realizations for a time interval where the network is in saturation stage.

For a network with BSs equipped with dipole antennas, the different array topologies have been investigated by simulations for a varying element number M. Fig. 8 shows that for all investigated array topologies, the network capacity, i.e. the average number of servable users, increases nearly linearly with the number of elements in the array M.

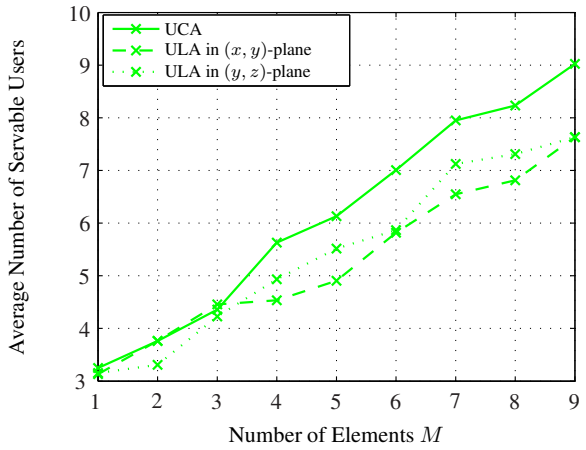

Fig. 8. Average number of servable users per cell versus the number of elements in the array for an array consisting of dipole antennas and different array topologies.

Furthermore, the UCA outperforms the ULA with increasing number of antenna elements M. In [2], this behaviour have been also found for a simplified static two-dimensional scenario. The ability of the ULA in the (y, z)-plane to perform additional beamforming in elevation direction tends to result only in a neglectable small performance gain compared to the ULA located in the (x, y)-plane. Since the users are equally distributed in the network with a cell radius of $r = 1$ km, most of the users are located at positions with a distance to the base station $d_{\mathrm{MS}\leftrightarrow\mathrm{BS}}$ which is much larger than the difference in height of the base station h_{BS} compared to the height of the user h_{MS}.

$$d_{\mathrm{MS}\leftrightarrow\mathrm{BS}} \gg (h_{\mathrm{BS}} - h_{\mathrm{MS}}) \tag{12}$$

Hence, the elevation angle for the paths to most of the users is close to $\theta = 90°$ such that additionally beamforming in the elevation direction does not achieve significant capacity gain. In hot spots of cellular networks with a much smaller cell radius, the effect of the elevation angle becomes much more of interest.

To determine a reasonable value for the DTA for the sectorized antenna, simulations have been performed for different DTAs for a network where the BSs are equipped with a UCA consisting of 9 commercially available sector antennas. Fig. 9 shows, that the network capacity becomes maximum for DTAs in the range of 2°-5°. Hence, in all subsequent simulations, the DTA of the sector antenna and the non-sectorized antenna with realistic DTA is set to 5°, since this value results in an adequate coverage of the network with a cell radius $r = 1$ km.

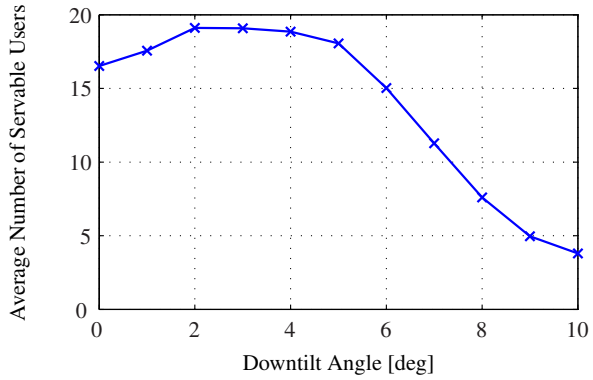

Fig. 9. Average number of servable users per cell for an UCA consisting of 9 commercially available sector antennas versus the antenna downtilt angle.

Using this DTA, the impact of three different array topologies has been examined by simulations for a network where the BSs are equipped with either sectorized antennas or non-sectorized antennas.

The simulation results shown in Fig. 10 and Fig. 11 for these antenna types confirm the discussed results for dipole antennas.

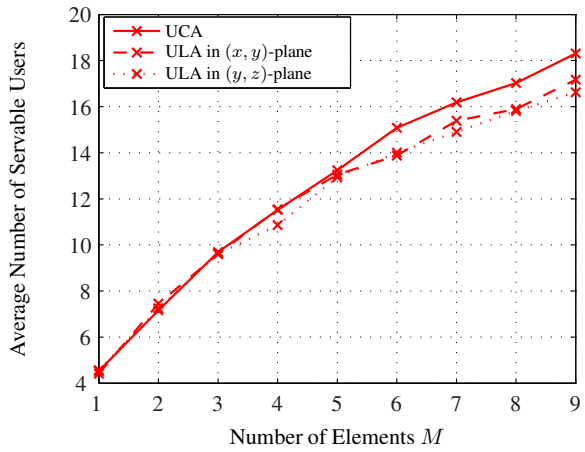

Fig. 10. Average number of servable users per cell versus the number of elements in the array for an array consisting of non-sectorized antennas with realistic downtilt angle and different array topologies.

Again, the network capacity increases almost linearly with the number of antennas in the antenna array while the UCA

outperforms the ULAs for all types of antennas. Furthermore, the ULA results in similar capacity gains for both orientation of the ULA (either (x, y)-plane or (y, z)-plane).

The capacity of a network equipped with a UCA is shown for all investigated types of antennas in Fig. 12. The sector antenna outperforms the dipole antenna due to its higher antenna gain. The reason is that the influence of thermal noise in the network becomes dominant for networks with low gain base station antennas.

Using non-sectorized antennas with realistic downtilt angle achieves capacity values close to the resulting capacity values which are obtained by using sector antennas. The high backward attenuation of sectorized antennas directly reduces the interference power in the network even though only a lower number of elements can be effectively used for beamforming due to the half-power beamwidth. Fig. 12 illustrates additionally that the network capacity increases approximately linearly with the number of antenna elements for all investigated types of antennas. It can be observed, that for each type of antenna doubling the number of the elements in the array results in approximately 50 % gain of the network capacity.

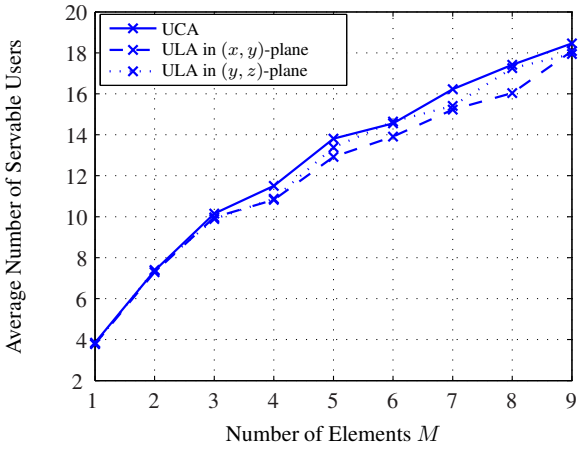

Fig. 11. Average number of servable users per cell versus the number of elements in the array for an array consisting of sectorized antennas and different array topologies.

7. CONCLUSIONS

The effect of different antenna elements in circular as well as linear arrays has been analysed for a UMTS-FDD network using simulations. A generalized antenna model has been presented which allows to investigate the impact of an array with arbitrary antenna characteristics as well as arbitrary element position and alignment for an entire cellular network. Simulation results show, that the uniform circular array achieves highest capacity in comparision with linear array concepts. Furthermore, the capacity of a cellular network

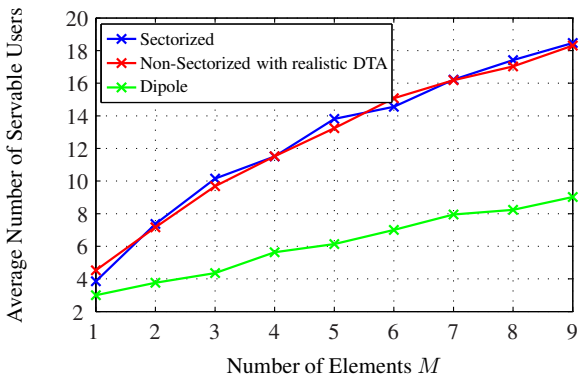

Fig. 12. Average number of servable users per cell for an UCA versus the number of elements in the array for the investigated antenna types.

increases almost linearly with the number of antennas in the antenna array. For a large cell radius, antenna elements with a small half-power beam width in elevation direction result in higher capacity compared with low-directional antennas like dipoles. Additionally, beamforming in the elevation direction increases the network capacity for the investigated cell size only marginally . Future works will concentrate on the deeper investigation on the impact of the half-power beam width in elevation as well as azimuth direction. A sectorization of the network cells will be implemented in the analysis.

8. REFERENCES

[1] J. C. Liberti, and T. S. Rappaport, *Smart Antennas for Wireless Communications: IS-95 and Third Generation CDMA Applications*. Prentice Hall, New Jersey, 1999

[2] A. Czylwik, and A. Dekorsy, *System-Level Performance of Antenna Arrays in CDMA-Based CellularMobile Radio Systems* EURASIP Journal on Applied Signal Processing, 2004

[3] L. Häring, B. K. Chalise and A. Czylwik, *Dynamic System Level Simulations of Downlink Beamforming for UMTS FDD*. In Proc. IEEE Global Conference on Communications, San Francisco, Dec. 2003.

[4] C. A. Balanis, *Antenna Theory*. John Wiley & Sons, New Jersey USA 2005.

[5] B. K. Chalise , L. Häring, and A. Czylwik, *Uplink to Downlink Spatial Covariance Transformation for Downlink Beamforming*. In Proc. IEEE VTC Spring 2004, Milan Italy, May. 2004

[6] C. Farsakh and J. A. Nossek, *Spatial Covariance Based Downlink Beamforming in an SDMA Mobile Radio System,*. In IEEE Trans. Vehicular Technology, vol. 48, pp. 333-341, 1999.

[7] Kathrein, *Radiation patterns for mobile communication antennas*. http://www.kathrein.de, 2005.